Environmental Pollution 240 (2018) 286–296

Contents lists available at ScienceDirect

Environmental Pollution

journal homepage: www.elsevier.com/locate/envpol

Sources and atmospheric processing of size segregated aerosol particles revealed by stable carbon isotope ratios and chemical speciation☆

A. Masalaite [a], R. Holzinger [b], D. Ceburnis [c], V. Remeikis [a], V. Ulevičius [a], T. Röckmann [b], U. Dusek [b, d, *]

[a] State Research Institute Center for Physical Sciences and Technology, Vilnius, Lithuania
[b] Institute for Marine and Atmospheric Research Utrecht (IMAU), Utrecht University, The Netherlands
[c] School of Physics & Ryan Institute's Centre for Climate and Air Pollution Studies, National University of Ireland Galway, Galway, Ireland
[d] Centre for Isotope Research (CIO), University of Groningen, Groningen, The Netherlands

ARTICLE INFO

Article history:
Received 25 October 2017
Received in revised form
4 April 2018
Accepted 16 April 2018
Available online 8 May 2018

ABSTRACT

Size-segregated aerosol particles were collected during winter sampling campaigns at a coastal (55°37′ N, 21°03′E) and an urban (54°64′ N, 25°18′ E) site. Organic compounds were thermally desorbed from the samples at different temperature steps ranging from 100 °C to 350 °C. The organic matter (OM) desorbed at each temperature step is analysed for stable carbon isotopes using an isotope ratio mass spectrometer (IRMS) and for individual organic compounds using a Proton Transfer Reaction Time-of-Flight Mass Spectrometer (PTR-MS). The OM desorbed at temperatures <200 °C was classified as less refractory carbon and the OM desorbed at temperatures between 200 °C and 350 °C was classified as more refractory carbon. At the coastal site, we identified two distinct time periods. The first period was more frequently influenced by marine air masses than the second time period, which was characterized by Easterly wind directions and continental air masses. During the first period OM contained a large fraction of hydrocarbons and had a carbon isotopic signature typical of liquid fossil fuels in the region. Organic mass spectra provide strong evidence that shipping emissions are a significant source of OM at this coastal site. The isotopic and chemical composition of OM during the second period at the coastal site was similar to the composition at the urban site. There was a clear distinction in source contribution between the less refractory OM and the more refractory OM at these sites. According to the source apportionment method used in this study, we were able to identify fossil fuel burning as predominant source of the less refractory OM in the smallest particles ($D_{50} < 0.18$ μm), and biomass burning as predominant source of the more refractory OM in the larger size range ($0.32 < D_{50} < 1$ μm).

1. Introduction

Aerosol particles have strong impact on the climate system, human health and visibility (Kaufman et al., 2002; Davidson et al., 2005). All these impacts depend on particle chemical composition and size. A significant fraction (~50%) of submicron aerosol particles is composed of organic matter (OM) (Jimenez et al., 2009; Putaud et al., 2010), which consists of thousands of individual compounds. Organic aerosol (OA) is either directly emitted into the atmosphere thus called 'primary' OA or formed though complex chemical reactions from gas phase precursors ('secondary' OA). However, finding accurate information about sources, composition and chemical processing of OM is challenging due to the variety of sources and the complexity of OM molecular composition. An even bigger challenge is understanding and predicting the size resolved OA composition and properties. Most previous studies of OA have focused on particulate matter <1 μm (PM_1), $PM_{2.5}$ (particulate matter <2.5 μm), or even PM_{10} (particulate matter <10 μm) but sources, health and climate effects of aerosols can differ strongly for different particle size ranges (Hueglin et al., 2005; Pérez et al.,

☆ This paper has been recommended for acceptance by Baoshan Xing.

* Corresponding author. Centre for Isotope Research (CIO), Energy and Sustainability Research Institute Groningen (ESRIG), University of Groningen, Groningen, The Netherlands.
E-mail address: u.dusek@rug.nl (U. Dusek).

https://doi.org/10.1016/j.envpol.2018.04.073
0269-7491/

2008; Górka et al., 2014; Bozzetti et al., 2016; Squizzato et al., 2016). Studies of even smaller aerosol particles ($PM_{0.5}$ and less) that have a major effect on human health are rare and more information on the size resolved OA composition and sources are needed.

Stable carbon isotopes can be used to study the sources and atmospheric processing of carbonaceous aerosol (Gensch et al., 2014). Previous research using the stable carbon isotopic composition of carbonaceous aerosol provided insight into sources (Cachier et al., 1985; Kawamura et al., 2004; Garbaras et al., 2008; Fisseha et al., 2009a; Masalaite et al., 2015; Bikkina et al., 2016), ranging from fossil fuel (FF) combustion to biogenic emissions from plants, as well as the extent of aerosol chemical processing in the atmosphere (Hegde et al., 2016; Ren et al., 2016; Sang et al., 2016; Zhang et al., 2016). Compound specific isotopic composition as well as stable carbon isotope ratios for the separate fractions of carbonaceous aerosol provide more detailed information on pollutants like individual fatty acids (Pavuluri and Kawamura, 2012; Zhang et al., 2016), or levoglucosan (Sang et al., 2012), water-soluble organic carbon (WSOC) (Kirillova et al., 2013), secondary organic aerosols (Saccon et al., 2015) or from combustion of biomass burning (BB) (Ballentine et al., 1998; Narukawa et al., 1999; Cao et al., 2011; Garbaras et al., 2015; Ulevicius et al., 2016). Previous studies in Lithuania (Masalaite et al., 2015) revealed that in the urban environment of Vilnius $\delta^{13}C$ values of the ambient aerosol could be explained by two main pollution sources (fossil fuel combustion and continental non-fossil). Fossil fuel combustion dominated in the production of fine aerosol particles ($D_p < 1.0$ μm) and had distinct stable carbon isotope ratio of -28.0 ± 0.1 ‰, which is typical of fossil fuel combustion in Eastern Europe (Górka and Jędrysek, 2008; Masalaite et al., 2012). The other source had a $\delta^{13}C_{TC} = -25.0 \pm 0.5$ and was attributed to a continental non-fossil source that was dominant in the coarse particle range ($1.0\ \mu m < D_p < 10\ \mu m$). Another study covering three different locations (urban, coastal and forest) showed that stable carbon isotope measurements can provide insight into effects of photochemical processing of the carbonaceous aerosol (Masalaite et al., 2017). The main obstacle in using stable carbon isotopes for carbon source apportionment is the overlap of the various source reference $\delta^{13}C$ values from various sources. Thus often the variation of the stable carbon isotope ratio in aerosol particles can be explained by a mix of several sources (Masalaite et al., 2015; Ceburnis et al., 2016) and additional measurements are required to solve mixing equations. Thus studies combining chemical and isotopic methods and a combination of various measurements are highly desirable.

Thermal desorption proton transfer reaction mass spectrometry (TD-PTR-MS) method is widely used to measure all kinds of organic compounds in the gas and aerosol phase (Hellén et al., 2008; Holzinger et al., 2010a; Holzinger et al., 2013; Inomata et al., 2014; Holzinger, 2015; Timkovsky et al., 2015). Due to using a quantitative, soft chemical ionization technique, PTR-MS shows relatively little fragmentation and allows tentative compound identification that helps interpreting the data received with stable isotope ratio mass spectrometer (IRMS) and the thermal–desorption isotope ratio mass spectrometer (TD-IRMS). The combination of the three methods of spectrometry (PTR-ToF-MS, IRMS and TD-IRMS) provides improved insights into source apportionment of carbonaceous aerosol as a function of particle size and thermal refractivity.

2. Experimental

2.1. Field campaign

The samples were collected at the coastal site Preila (Lithuania, 55°37′ N, 21°03′ E; 5 m above mean sea level) during winter of 2012 (November–December) and in the urban location of Vilnius city (Lithuania, 54°64′ N, 25°18′ E; 65 m above mean sea level) during winter of 2008–2009 (Table 1). A micro-orifice uniform deposition 11 stages impactor (MOUDI-110) was used for the collection of size-segregated samples and operated at a flow rate of 30 L/min. Aluminium foils of 47 mm in diameter pre-fired for 10 h at 600 °C were used as sampling substrates. The cut-off sizes of the impactor stages were as follow: 0.056, 0.1, 0.18, 0.32, 0.56, 1.0, 1.8, 3.2, 5.6, 10, 18 μm. This study presents the fine mode particle range ($D_{50} = 0.056–1.0$ μm) divided into three size ranges: $D_{50} < 0.18$ μm (the sum of the 0.056, 0.1 and 0.18 μm stages), $0.18 < D_{50} < 0.32$ μm (corresponds to the 0.32 μm stage) and $0.32 < D_{50} < 1$ μm (the sum of the 0.56 and 1 μm stages). The division into the three size ranges was supported by factor analysis performed with IBM SPSS statistical software (IBM, 2013) (supplementary material).

The aerosol particle number size distribution was measured using a scanning mobility particle sizer (SMPS, 19.3.09 IFT/TT model). The particle sizer consists of HAUKE-type medium differential mobility analyser (DMA), a condensation particle counter (CPC, UF-02M model) (Mordas et al., 2008), a radioactive neutraliser and a Nafion membrane dryer (Perma Pure LLC, MD-110-48S-4 model). The operational parameters of SMPS were: aerosol flow – 1.0 ± 0.2 L min^{-1}, sheath flow – 5.0 ± 0.1 L min^{-1}, and a positive voltage source varying from 0 to 10^4 V (Wiedensohler et al., 2012). The duration of each scan was 5 min. The aerosol particle size distribution was separated into 71 bins and ranged from 9 to 840 nm. Aerosol particles were neutralised by passing through a radioactive α-source containing ^{239}Pu. The particle diffusion losses were corrected using the Gormley-Kennedy equation for cylinder tube. The multiple charge correction was performed using the approximation of a bipolar charge distribution for lower charges (−2, −1, +1, +2) (Wiedensohler, 1988).

The Aethalometer (Magee Sci., AE-31 model) was deployed to measure aerosol particle light absorption properties and equivalent black carbon (BC) mass concentration at the coastal site. The optical attenuation was measured for seven wavelengths (λ 370, 450, 520, 590, 660, 880 and 950 nm). The standard value of BC mass concentration in the atmosphere is associated with the light attenuation at 880 nm (Kirchstetter and Novakov, 2007). The conversion of optical attenuation to BC mass concentration was done using the mass absorption cross-section value of 16.6 m^2 g^{-1} provided by the manufacturer. Empirical algorithms were used for the filter loading corrections (Weingartner et al., 2003; Virkkula et al., 2007).

Basic meteorological parameters at the coastal site such as air temperature, wind speed and wind direction were provided (Table 1) by the meteorological station 40 km to the north from the coastal aerosol sampling station (Fig. 1 (a)) for the period lasting from 2012 11 30 to 2012 12 17. However no meteorological parameters were available for the city site.

Air mass back trajectories were calculated using the National Oceanic and Atmospheric Administration (NOAA) HYSPLIT model (Stein et al., 2015). 72 h isobaric air mass back trajectories were computed at a height of 500, 100 and 50 m a.s.l. with a new trajectory starting every 6 h (Fig. S1). The difference between air mass direction at different altitudes (500, 100 and 50 m a.s.l.) was small thus the most representative figures are given in Fig S1 and Fig. 1 (a). Despite the location of the coastal site in the Curonian Spit National Park, local and regional pollution sources can influence aerosol particles collected at the coastal site. The aerosol sampling site is located 40 km south from the harbour - one of the potential pollution sources (Fig. 1 (a)). The samples of aerosol particles were divided into three episodes according to site and air mass direction. The air mass backward trajectories at the coastal site were from South, South West, West and North during the first three periods of sampling lasting from November 26 to December 09 of 2012. The

Table 1
Overview of the sampling durations and several parameters. Details on the calculation of average OA_{PTR}, BC time series, and air mass back trajectories are given in the supplemental material.

Sampling site	Duration of sampling	Dominant air mass	OA_{PTR}, μg/m^3	BC, μg/m^3	NPF	Average wind velocity, m/s	Dominant wind direction (time duration of the sector in %)
Coastal 1	2012 11 26; 24:00–2012 11 30; 12:00	S, SW	2.11	2.13	yes	–	–
	2012 11 30; 12:00–2012 12 04; 16:00	S, W, N	0.49	1.12	yes	1.24	SW (22), W (20), E (19)
	2012 12 04; 16:20–2012 12 09; 9:17	W, N (Clean)	0.90	2.02	yes	0.95	E (37), S (21), SW (11)
Coastal 2	2012 12 09; 10:09–2012 12 13; 10:00	N, E	0.91	1.86	yes	0.76	E (41), SE (27), SW (12)
	2012 12 13; 10:24–2012 12 17; 10:15	S, SE	0.61	1.28	yes	1.43	E (42), SE (16), SW (11)
City	2008 12 30–2009 01 07	N, NW, W	2.22	–	–	–	–
	2009 01 07-16	N, W	1.85	–	–	–	–
	2009 01 16-26	S, SE, E	1.12	–	–	–	–

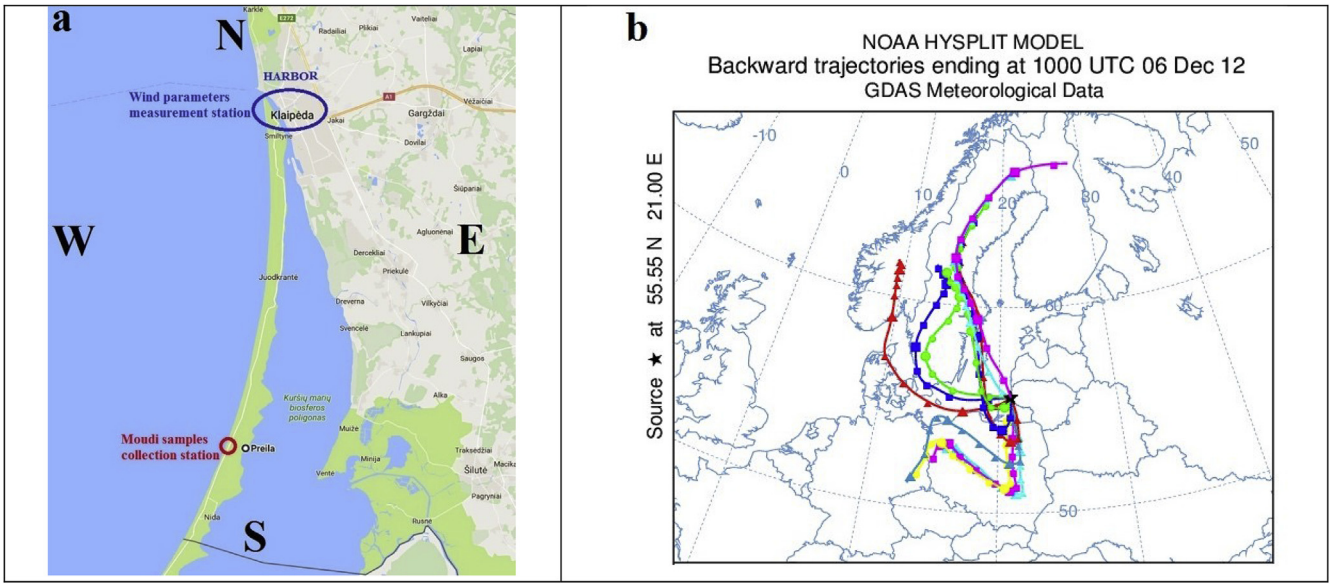

Fig. 1. Meteorological data collection site in harbour (a) (GoogleMaps, 2016) and Moudi samples collection site with typical for coastal 1 period air mass trajectories (b) (Stein et al., 2015).

main feature of these air masses was that they originated and/or advected over Baltic Sea, Atlantic Ocean and Scandinavia (supplementary material). The samples of the above period were combined and are referred to as coastal 1 period. The period from December 9 to December 17 of 2012 is referred to as 'coastal 2 period' and is characterized by dominant air masses from North, East, Southeast and South. These air masses had predominant continental origin and most advected over land (supplementary material). Meanwhile the air masses at the urban site were mixed, therefore, all three episodes (12 30 2008–01 26 2009) were combined and referred as to urban (Table 1). Fig. 1 (b) shows an example of 72-h air mass back trajectories ending 06 Dec 2012 during coastal 1 period at 100 m height.

2.2. Instrumentation

For chemical and isotopic analysis, the carbonaceous aerosol collected on the impactor stages was desorbed at different temperatures ranging from 100 to 350 °C in an inert atmosphere. While the desorption temperature is not a direct indicator of the particle volatility, it still provides a qualitative estimate of the organic matter refractivity. Carbonaceous material desorbed at lower temperatures (100–200 °C) is less refractory, whereas more refractory carbonaceous material desorbs at higher temperatures (250–350 °C).

2.3. TD_PTR-ToF-MS

The chemical composition at each temperature step was determined using a Proton Transfer Reaction Time-of-Flight Mass Spectrometer (PTR-ToF-MS) (Holzinger et al., 2010b) for 20 samples of coastal 1 period (and 3 blanks), 17 samples of coastal 2 period (and 3 blanks) and 43 samples of city site (and 6 blanks). The number of replicas varied from 1 to 3 depending on the amount of material collected on each impactor stage. The measured size range was $D_{50} = 0.056–1.0$ μm (the cut-off sizes of the impactor stages 0.056, 0.1, 0.18, 0.32, 0.56, 1.0).

The detailed description of PTR-ToF-MS measurements is provided by Masalaite et al. (2017). In short, the aluminium foil sample was introduced into an oven (similar to the IRMS system described below) and flushed with N_2 for 2 min. The organic compounds were evaporated in pure N_2 flow by increasing the temperature from 100 °C to 350 °C in steps of 50 °C, lasting 180 s each. Condensation of the volatilized gasses was avoided by keeping the second part of the oven at constant 200 °C temperature. A fraction of the flow was subsampled for the PTR–MS measurement from the second part of the oven.

The operating conditions during the measurements with the PTR–MS were as follows. The temperature of the drift tube was 117 °C and the temperature of the inlet line was 180 °C. The voltage across the drift tube (U_d) was 600 V and the voltage at the end of

the drift tube (U_{dx}) was28 V. The pressure (2.8 mbar) in the drift tube, the voltage (140 V) and the current (4–5 mA) of the ion source were constant. The intensity of the primary protonated water ion signal, that was calculated from the signal at m/z = 21.023, was detected at more than 2.5 $\cdot 10^5$ cps (count per second). ToF mass resolution based on Full Width at Half Maximum (FWHM) varied from 3000 to 3500.

The evaluation of the raw data was made using Interactive Data Language (IDL, version 7.0.0, ITT Visual Information Solutions) with custom-made routines described by Holzinger (2015). In short, 975 organic species were identified by the mass to charge ratio (m/z). Initially, the measured concentrations were reported as volume mixing ratios of the compounds in the N_2 carrier gas in nmol/mol multiplied by one second [s·nmol/mol]. The mixing ratios are calculated directly from the (i) ratio of the signals of the respective mass peaks and the primary H3O ions, (ii) default reaction rate constants for exothermic proton transfer reactions and (iii) instrumental parameters, as detailed in Holzinger et al. (2010b). The volume mixing ratios are converted to ambient air concentrations [ng/m^3] as detailed in Masalaite et al. (2017). A unified mass list was compiled from all the detected compounds. Molecular formulas from a previously determined mass library (Holzinger et al., 2010a; Holzinger, 2015) were assigned to the individual masses from the list as described in detailed by Timkovsky et al. (2015) and Masalaite et al. (2017). Several compounds (out of 975) were excluded due to association with inorganic ions related to nitrate (m/z = 45.99 and 46.00) and all ions with m/z values below 40 D_a except m/z 27.022, 31.017, 32.049, and 33.034, which were attributed to $C_2H_3^+$, CH_2OH^+, CH_5NH^+, and CH_4OH^+ respectively. Also ions for which the blank accounted for more than 70% of the signal and ions clearly associated with contamination (>1000 nmol/mol on the blank) were excluded from further analysis. 907 ions were left for data analysis after careful examination of the dataset. The sum of the mass concentration of all ions gives concentration of collected organic matter (in units of ng/m^3 or μg/m^3) for each impactor stage and temperature step. This will be referred to as OA_{PTR} in the remainder of the manuscript. In a first analysis step, the OA_{PTR} is summed over volatility classes (100–200 °C: less refractory and 250–350 °C: more refractory). The total OA in each volatility class could be sub-divided according to the attributed chemical formula into five classes: C_xH_x (hydrocarbons), $C_xH_xO_x$ (oxygenated hydrocarbons), $C_xH_xN_x$ (nitrogen containing hydrocarbons), $C_xH_xO_xN_x$ (ions containing carbon, hydrogen, oxygen and nitrogen) and Z (unidentified compounds). Another subdivision was according to m/z ranges (m/z < 100, 100 < m/z < 200 and m/z > 200). In a second step the OA was summed over the three size ranges specified above. The total OA_{PTR} is the sum over all temperature steps and impactor stages. Finally the average OA for samples taken during episodes at a given site (coastal 1, coastal 2 and urban) was calculated in the three size ranges and volatility fractions. More details about the calculations of average concentrations can be found in the supplementary material, section 5. The standard deviations corresponding to these sample averages typically varied from 1 to 47% with an average of 30%. The highest standard deviation (an outlier values of 149%) was at the 100 °C temperature step where the detected OA_{PTR} mass (particularly for $C_xH_xO_xN_x$ ions) is lowest and contamination from sampling and handling can have a large influence on the measured values.

In the same way averages of the O/C and H/C ratios were calculated for the different size ranges and volatility classes by summing up all the O, C, and H over the respective impactor stages and temperature steps, and then divided O/C and H/C for each volatility class and size class and finally averaged it over the site/period. The standard deviation of O/C and H/C varied from 3.3 to 24.6% and from 0.6 to 4.6% of the value respectively.

2.4. IRMS

Stable carbon isotope ratios were measured for the organic carbon (OC) fraction at different desorption temperatures and for the total carbon (TC) of size segregated aerosol samples. Carbon isotope ratios ($\delta^{13}C$) for TC deposited on the aluminium foil samples were measured using an elemental analyser (Flash EA1112; Thermo Delta V Advantage, Thermo Scientific, USA) connected to the stable isotope ratio mass spectrometer (IRMS) Thermo Delta V Advantage, following the analytical procedure detailed in Ceburnis et al. (2011). $\delta^{13}C_{TC}$ values were blank corrected using the isotope mixing equation. Duplicate samples were analysed and the reproducibility of $\delta^{13}C_{TC}$ measurements was estimated as the standard deviation of the $\delta^{13}C_{TC}$ measurements (n = 2). The reproducibility of $\delta^{13}C_{TC}$ was in the range of 0.2‰.

For $\delta^{13}C_{OC}$ measurements, aluminium foil samples are introduced into an oven, where organic compounds are thermally desorbed in helium at different temperatures (Dusek et al., 2013). The thermal–desorption isotope ratio mass spectrometry (TD-IRMS) system consisted of a quartz glass tube surrounded by two ovens which was coupled to an isotope ratio mass spectrometer. A sample was introduced into a first oven at room temperature. The temperature of a first oven was increased from 100 °C to 400 °C in steps of 50 °C while the second oven was kept at constant temperature (550 °C). Organic compounds were desorbed in a flow of pure helium for 7 min at each temperature step. A Platinum catalyst was used in the second oven to oxidize the desorbed organic compounds to CO_2. Two consecutive liquid nitrogen traps were used for concentration and purification of received carbon dioxide. A gas chromatography column (Varian CP351) was used to separate CO_2 from possible traces of NO_2 and N_2O. Water vapour was removed with a Nafion dryer. Consequently, only pure carbon dioxide entered the IRMS via a custom-made open split interface (Röckmann et al., 2003). All $\delta^{13}C$ ratios are reported relative to the Vienna Pee Dee Belemnite (VPDB) standard.

The isotope mixing equation was used for blank correction of the measured the $\delta^{13}C_{OC}$ values at each desorption temperature step. The $\delta^{13}C_{OC}$ values of the blank foils were determined on two (for urban site) and three (for coastal site) blank aluminium foils that were treated like the sample foils except that no aerosol was collected on them. For each sample the blank correction was done several times, using values for the individual blank foils (2 for urban; 3 for coastal) and the corrected $\delta^{13}C_{OC}$ values were averaged. The standard deviation in $\delta^{13}C_{OC}$ after correction ranged from 0.00 to 0.24. $\delta^{13}C_{OC}$ values were determined using a single aluminium foil piece for most of the stages, due to the limited material available. Reproducibility tests of $\delta^{13}C_{OC}$ averaged over all temperature steps were performed on two foils from coastal site and revealed reproducibility for $\delta^{13}C_{OC}$ averaged over all temperature steps of around 0.5‰.

The value of $\delta^{13}C_{OC}$ for each size range ($D_{50} < 0.18$ μm, $0.18 < D_{50} < 0.32$ μm and $0.32 < D_{50} < 1$ μm) was calculated as average over the representative impactor stages with standard deviations ranging from 0.04 to 1.05‰ with an average of 0.41‰. The averaged value of $\delta^{13}C_{OC}$ of each volatility class was calculated using the average of the size range and averaging over desorption temperatures (100–200 °C and 250–350 °C). The average of standard deviations was 0.38‰.

3. Results and discussion

The OM collected on coastal 1 and coastal 2 samples had different O/C ratios, $\delta^{13}C_{OC}$ values and for some time periods

different black carbon (BC) concentrations (Table 1). During the coastal 1 period, characterized by more frequent air mass back trajectories from the marine sector, the O/C ratio was low (0.22–0.24) and stable carbon isotopic composition was strongly negative with an average of $\delta^{13}C_{OC} = -29.4 \pm 0.3$‰. BC concentrations alternated between very clean periods with BC concentration <0.5 μg/m^3, and very polluted periods with concentrations ranging from 3 to 6 μg/m^3. On the other hand for the coastal 2 period O/C ratios increased to an average of 0.34, BC concentrations were less variable and mostly between 1.5 and 3 μg/m^3 and $\delta^{13}C_{OC}$ was -26.6 ± 0.1‰, enriched in ^{13}C in comparison to coastal 1. More detailed information is given in supplementary material (Fig. S2).

Black carbon concentrations can give an indication about possible pollution plumes from nearby sources. Fig. 2 shows BC concentrations (right axis) as a function of local wind direction at the coastal site. For the coastal 1 time period the highest BC concentrations were associated with wind directions from N, NE, S and SE (hourly average reaching up to 5.70 μg/m^3) and much lower concentrations with wind directions from SW and W. Note that the local wind direction can be different (even opposite) to the large scale synoptic flow (revealed by air mass trajectories). The air mass trajectories were from South and South West during the highest BC loadings. A large-scale westerly air flow brings clean air therefore the impact of local pollution sources (nearby the sampling site, e.g., when the local wind direction is from the harbour location) is more evident. In contrast, no specific relationship was found between BC concentration and wind direction during the coastal 2 time period (Fig. 2). This may be due to the large-scale air mass from the land that advected over the ocean. In that case, local wind direction was not so important, because of relatively homogeneous aerosol concentrations due to long-range transport in the region.

Aerosol samples from the coastal 1 period can locally be influenced by shipping emissions as the studies of ship emissions in coastal areas suggest (Viana et al., 2014; Di Natale and Carotenuto, 2015), as well as by pollutants from Klaipeda harbour (mixed shipping and urban emissions). It is also possible that coastal 1 samples can be affected by advection of aged and photo-chemically processed PM from inland regions transported by the prevalent air trajectory crossing neighbouring countries. Russia – Kaliningrad region is located 80 km to the South from the sampling location and Poland, well-known for high coal combustion pollution (Rogula-Kozłowska et al., 2014), is also in the South (South-West). In general, the coastal 1 period showed very clean conditions alternating with strong, possibly local pollution plumes. Since the clean time periods contribute little mass to the total organic carbon collected on the impactor samples, the integrated samples are consequently primarily representative of these local pollution sources.

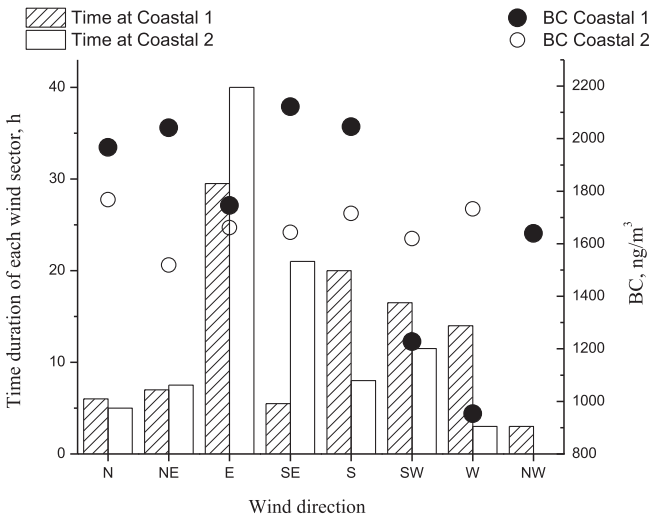

Fig. 2. Time duration of the wind sector (left axis) and corresponding BC concentrations (right axis) at coastal site.

OA_{PTR} collected on the individual impactor stages samples ranged from 0.17 μg/m^3 during coastal 2 to 0.63 μg/m^3 at the urban site. The contribution of various chemical classes (CH, CHO, CHN, CHON and unidentified compounds) to the measured mass concentration differed between the sites. The largest difference was for hydrocarbons (CH), which accounted for ~23% in coastal 1 samples, but only 7% in urban samples. The highest contribution to OA_{PTR} was from CHO ions, ranging from 48% (coastal 1) to 60% (urban) of the analysed organic mass. CHON ions composed 17% of OA in coastal 1, 22% in costal 2 and 25% at an urban site. The smallest fraction, CHN ions, accounted only for 2–4% of OA_{PTR} in all sites.

The OA fraction at different desorption temperatures is shown in Fig. 3. For coastal 2 60% of the OA is less refractory and 40% of OA is more refractory for all size ranges. There is an indication, that the contribution of less refractory carbon is higher for coastal 2 than for the urban site and costal 1. Aerosol particles in the size range of $0.32 < D_{50} < 1$ μm at coastal 1 exhibited the highest percentage (almost 60%) of more refractory OA (or OM).

Fig. S3 provides an overview of the PTR-MS mass spectra at low and high desorption temperatures at different locations. Again the coastal 1 period was exceptional and differed strongly from the other samples, whereas the mass spectra of the urban site and the coastal 2 period are more similar. OA_{PTR} mass spectra in the two desorption temperature ranges revealed high mass concentration of heavy ions (m/z > 300) at the coastal 1 site (Fig. S3). They showed a distinctive regular pattern and were the most pronounced in the more refractory OA. To shed more light on the composition of the more refractory OA at the three sites, the ions with the highest concentrations for m/z > 300 are listed in (Table S3). Most of the highest peaks visible in Fig. S3 for coastal 1 are found in the largest particle size range and can be attributed to oxygenated long-chain alkanes (e.g. m/z 385.38, 357.34) or hopanes (e.g., 399.39, 369.35) (Lambe et al., 2009) (Table S3), which points to a fossil fuel origin of these compounds. The chemical composition in the larger particles

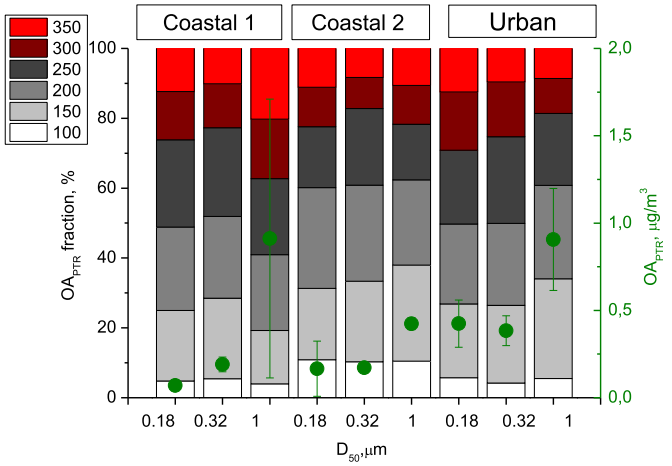

Fig. 3. Thermograms of ambient OA_{PTR} samples collected at coastal and urban sites (the monthly averaged values). The x axis labels 0.18, 0.32 and 1 refer to $D_{50} < 0.18$ μm, $0.18 < D_{50} < 0.32$ μm and $0.32 < D_{50} < 1$ μm, respectively. The sum of OA_{PTR} mass of each T step is marked in dots (the right axis). Details on the calculation of the average OA_{PTR} and OA_{PTR} fraction for each period are given in the supplementary material. Error bars correspond to the standard deviation of mean of the samples averaged for each period.

size range shows similarities between the 2 coastal periods, as a number of the most prominent compounds for coastal 1 are also present in the coastal 2 samples (m/z 385.38, 371.36, 399.39, 387.39, 369.35), albeit at much lower concentrations. None of these compounds are present in the top ten compounds at the urban site, which suggests that this pollution source is related to the coastal site, and contributes much more strongly to the samples of the coastal 1 period. The above distinctive patterns were also broadly identified by the SPSS PC analysis, however, were only indicative and not strictly defined, especially for the components explaining relatively smaller amount of the total variance (components 2 and 3) as compared to the component 1.

In contrast, the more refractory OA at the smallest particle size is much more similar between the three sites and dominated by highly oxidized molecules. For the urban and coastal 2 samples, particles in the intermediate size range have a very similar organic composition as the smallest size range. For the coastal 1 samples the most prominent compounds are a mixture of hydrocarbons found primarily in the large particle size range and the highly oxidized compounds found primarily in the smallest particle size range. Fig. S3 indicates that more refractory OA contains more heavy compounds (with $m/z > 300$) than less refractory OA. Compounds with $m/z > 300$ contribute only 10% to the less refractory OA fraction ($T = 100–200\,^{\circ}C$), but 20% to the more refractory OA section for the urban site and the coastal 2 period. In contrast, for coastal 1 samples compounds with $m/z < 300$ contribute 60% to the less refractory OA and 70% to the more refractory OA. The mass spectra of the coastal 1 and coastal 2 samples were somewhat similar for $m/z < 250$ except that in coastal 1 there was little mass in the smallest particles range. If the coastal 1 period was dominated by local pollution, this suggested that local source emitting relatively large particles and heavy organic compounds ($m/z > 300$). In summary, chemical analysis shows a strong contribution of heavy hydrocrabons to particles in the size range between 0.18 and 1 μm during coastal 1 and to a much lesser extent during coastal 2. The high variability in BC concentrations during the same coastal 1 time period suggests a local/regional source, probably related to harbour (Viana et al., 2014) or shipping related emissions (Worton et al., 2014; Eichler et al., 2017).

In Fig. 4 (a) coastal 1 organic mass spectra are compared to the mass spectra of ship emissions analysed with a proton-transfer-reaction time-of-flight mass spectrometer by Eichler et al. (2017). On Y axis is relative concentration that denotes the mass received from the PTR-ToF-MS measurements. Relative concentration denotes OA_{PTR} in ng/m^3 for aerosol particles measured in coastal 1 samples whereas the concentrations measured in heavy fuel oil exhaust (HFO) by Eichler et al. (2017) were reported in count rates that were normalized to 10^6 $(H_2O)_{1,2}H^+$ reagent ions and are shown in units of normalized counts per second (ncps) multiplied by m/z and divided by 1000. Details on the qualitative and quantitative interpretation of the obtained mass spectra of HFO exhaust particles are given in the Supporting Information by Eichler et al. (2017). The ions identified in the mass spectra of the shipping emissions account for 59% of the total OA_{PTR} of the more refractory OM in the size range $0.32 < D_{50} < 1$ μm (Fig. 4 (a)). Fig. 4 (b) shows a scatter plot between the mass concentration of individual ions found in the more refractory OM ($0.32 < D_{50} < 1$ μm) collected during coastal 1 period and the count rate of heavy fuel oil exhaust particles measured by Eichler et al. (2017). High correlation ($r = 0.96$) at $m/z = 400–554$ (Fig. 4 (b)) reveal the similarities between both mass spectra. The highest signals of coastal 1 period and HFO mass spectra were the same $m/z = 371.37$ ($C_{27}H_{46}H^+$); 385.38 ($C_{24}H_{48}O_3H^+$); 399.40 ($C_{29}H_{50}H^+$); 387.40 ($C_{24}H_{50}O_3H^+$); 397.38 ($C_{29}H_{48}H^+$); 413.42 ($C_{30}H_{52}H^+$); 411.40 ($C_{30}H_{50}H^+$). It is worth noting that molecular formulas from a determined mass library list were assigned according to the rules explained in methodology section but usually the choice of attributing the formula was more than one ion. In case of $m/z = 385.38$ it is also possible to have a hydrocarbon $C_{28}H_{48}H^+$ as well as in $m/z = 387.40$ case ($C_{28}H_{50}H^+$). Eichler et al. (2017) attributed the mentioned peaks mainly to unburned lubricating oil. This could be an explanation, why the $\delta^{13}C_{OC}$ of the samples from coastal 1 period approaches the values of unburned fossil fuels, especially for the less refractory OA fraction. However, direct measurements of the $\delta^{13}C$ of lubricating oil used in Eastern Europe are not known to us. The H/C ratio of ions with $m/z > 300$ reached up to 2.08 and the O/C ratio of 0.13 is typical to the fossil fuel emissions (Collier et al., 2015).

It is worth noting that some of the detected signals at all sites ($m/z = 149.02$, 257.24, 199.04, 203.08) showed significant similarities to the mass spectra measured in a Tunnel study of Brazil (Oyama et al., 2016). In that study ion with $m/z = 149.02$ ($C_8H_4O_3H^+$) was tentatively attributed to phthalic anhydride and is well known for its use as plasticizers and also present in the plastic bags. The plastic bags are used for storage of the collected filters wrapped in aluminium foil. Thus this ion may be associated with contamination from plastic bags. However, on the blank filter the mass concentration of m/z 149.02 is low (0.08 ± 0.05 ng/m^3), on the filters from the coastal site it is on average 5.9 ± 3.9 ng/m^3 and on

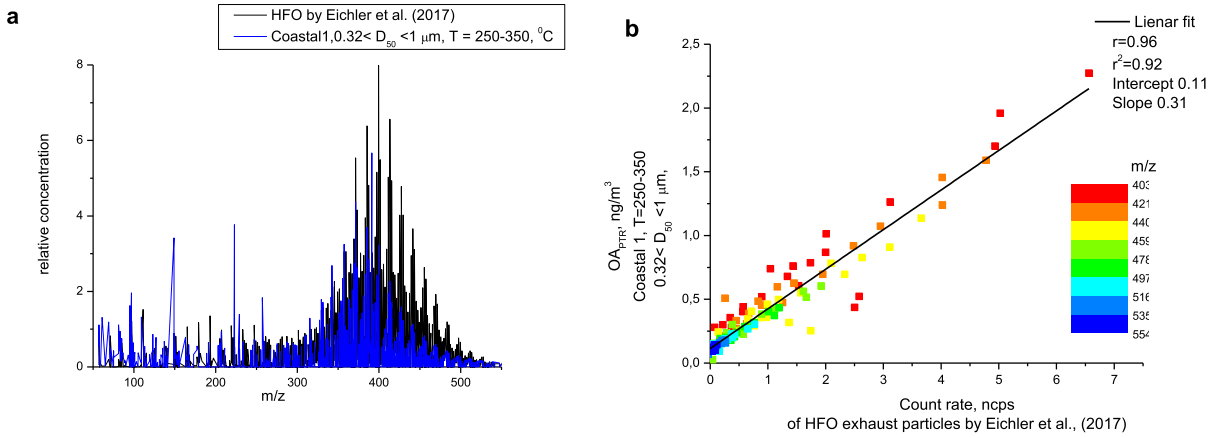

Fig. 4. The organic mass spectra obtained by a proton-transfer-reaction time-of-flight mass spectrometer in coastal 1 samples and heavy fuel oil exhaust particles from ship engine by Eichler et al. (2017) (a, left). The correlation of more refractory aerosol particles collected during coastal 1 period in size range of $0.32 < D_{50} < 1$ μm (measured in ng/m^3) and HFO exhaust particles (measured in ncps) by Eichler et al. (2017) at $m/z = 400–554$ (b, right).

the filters from the urban site it is 8.5 ± 6.1 ng/m^3. Such difference in mass concentration suggests that it is not an artefact but present in the atmospheric samples. Oyama et al. (2016) suggest that phthalic anhydride may be produced from tire wear and Al-Naiema and Stone (2017) found that phthalic acid could be from oxidation of polycyclic aromatic hydrocarbons or primary emissions (motor vehicle engines, aromatic volatile organic compounds).

A summary of $\delta^{13}C$ and O/C, H/C ratios are given in the Table 2 for the different size and volatility classes. Usually OA in the less refractory fraction had lower O/C and lower $\delta^{13}C$ ratios than OA in the more refractory fraction, especially in the smaller particle size ranges ($D_{50} < 0.32$ μm). H/C ratios are lower in the more refractory than in the less refractory OA in coastal 1 samples, but are relatively comparable in both volatility fractions at the other two sites. The averaged O/C ratio was smallest in coastal 1 site (0.20) and highest in urban site (0.45). An opposite trend was observed for H/C ratio: it was smallest in urban samples (1.25) and highest in coastal 1 samples (1.44). The increase of $\delta^{13}C$ and O/C for the less refractory carbon may be associated with the relative source contribution of biomass burning (BB) and fossil fuel (FF) combustion. Fossil fuel emissions are depleted in $\delta^{13}C$ and less oxidized compared to typical biomass burning sources in Lithuania. Fossil fuel burning produces on average less refractory carbonaceous aerosol than biomass burning, which is consistent with enriched $\delta^{13}C$ and higher O/C ratios in the more refractory OM. However, enrichment of $\delta^{13}C$ can also be a result of atmospheric processing, but evidence for this process in winter was mainly found at a remote forest site (Masalaite et al., 2017). In summer, however, factors like higher radiation, temperature and OH/O_3 concentrations can lead to more enriched $\delta^{13}C_{TC}$ values also in other locations.

Fig. 5 presents $\delta^{13}C_{OC}$ ratios at two desorption temperatures ranges (100–200, 250–350 °C) for three aerosol particles size ranges (D_{50} up to 0.18, 0.32 and 1 μm). The variability of the stable carbon ratio in size-segregated aerosol particles (from −30.9 ‰ to −25.1‰) suggested various sources of aerosol particles contributing to carbonaceous particulate matter in different locations. Previous studies have demonstrated that anthropogenic aerosols during winter in Lithuania are mostly produced by fossil fuel combustion and biomass burning (Masalaite et al., 2015; Garbarienė et al., 2016). Typical $\delta^{13}C_{TC}$ values related to these sources are represented by shaded area in Fig. 5. The green line represents $\delta^{13}C_{TC}$ of biomass waste pellets (−25.1 ± 0.2‰ (Garbaras et al., 2015)), which are a common commercially available biomass fuel in Lithuania. This value is close to an enriched in ^{13}C background source ($\delta^{13}C_{TC}$ ~ −25 to −26‰) in Lithuania that was identified in a previous studies and attributed mainly to biomass burning (Garbaras et al., 2015) with some contribution from coal combustion (Widory, 2006) during winter time (Masalaite et al., 2015; Garbarienė et al., 2016). This $\delta^{13}C_{TC}$ is in good agreement with the average value of $\delta^{13}C_{TC}$ of biomass burning aerosols

Table 2
The summary of stable carbon measurements at different sites, size ranges and desorption temperatures. Details on the calculation of average $\delta^{13}C$, O/C, and H/C ratios for the different size and temperature ranges are given in the supplementary material. +/− uncertainty ranges correspond to the standard deviation of mean of the samples averaged for each period. Typical reproducibility for$\delta^{13}C_{TC}$are 0.2‰.Reproducibility of individual $\delta^{13}C_{OC}$ values are roughly 0.5‰, the uncertainty of the averages of three values is roughly a factor of 1.7 [= sqrt(3)] smaller than this (approx. 0.3‰).

T, ^{0}C			1020	350	100–200	250–350	100–200	250–350	100–200	250–350
Sampling site	Air mass	D_{50}, μm	$\delta^{13}C_{TC}$	$\delta^{13}C_{OC}$, ‰	$\delta^{13}C_{OC}$, ‰	$\delta^{13}C_{OC}$, ‰	O/C	O/C	H/C	H/C
Coastal 1	N, S, W	0.32 < d < 1	−28.1	−29.9	−30.7	−29.1	0.20	0.20	1.44	1.38
		0.18 < d < 0.32	−27.3	−29.0	−29.6	−27.3	0.24	0.30	1.37	1.32
		<0.18	−27.9	−28.6	−29.4	−27.9	0.26	0.35	1.35	1.30
Coastal 2	N, E, S	0.32 < d < 1	−25.5	−26.3	−26.7	−25.6	0.30	0.30	1.33	1.34
		0.18 < d < 0.32	−26.1	−27.0	−26.9	−26.6	0.32	0.44	1.31	1.26
		<0.18	−25.9	−26.9	−27.0	−26.7	0.31	0.33	1.34	1.32
City	N, E, S, W	0.32 < d < 1	−25.6	−25.7	−26.2	−25.3	0.34	0.37	1.26	1.28
		0.18 < d < 0.32	−26.1	−26.1	−26.3	−25.9	0.35	0.45	1.26	1.25
		<0.18	−26.3	−26.7	−27.0	−26.4	0.36	0.40	1.26	1.26

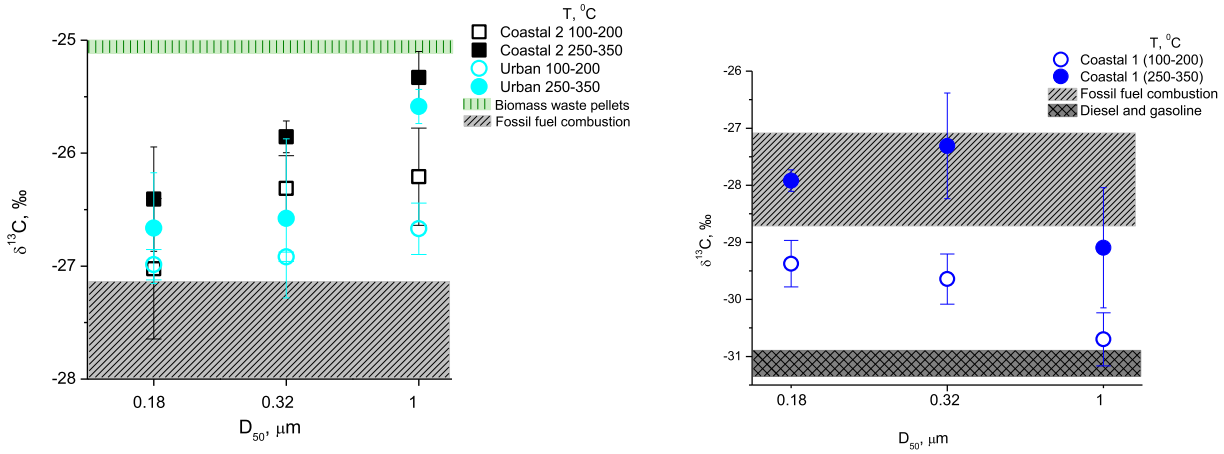

Fig. 5. An overview of the isotopic composition of OC via VPDB at urban (squares) and coastal (circles) sites for size segregated aerosol particles in two desorption temperature ranges (100–200, 250–350 °C). The lines give rough indications of the isotopic composition (TC) via VPDB of biomass waste pellets (green), fossil fuel combustion (grey) and raw diesel and gasoline $\delta^{13}C_{TC}$ values (dark grey). Notation of x axis 0.18, 0.32 and 1 are $D_{50} < 0.18$ μm, $0.18 < D_{50} < 0.32$ μm and $0.32 < D_{50} < 1$ μm, respectively. Error bars correspond to the standard deviation of mean of the samples averaged for each period. Reproducibility of individual $\delta^{13}C_{OC}$ values are 0.5‰, the uncertainty of the averages of three values is roughly a factor of 1.7 [= sqrt(3)] smaller than this. (For interpretation of the references to colour in this figure legend, the reader is referred to the Web version of this article.)

reported by Kundu et al. (2010), but a bit more depleted compared to biomass burning values reported by Cao et al. (2016) (−24.2‰). The light grey area gives a possible range of $\delta^{13}C_{TC}$ value for particles produced by fossil fuel combustion ($\delta^{13}C_{TC} = -28 \pm 0.9$‰) in Eastern Europe. The $\delta^{13}C_{TC} = -31.2 \pm 0.2$‰ value typical for raw diesel and gasoline fuel in Lithuania (Masalaite et al., 2012) is shown with dark grey line.

In the urban and coastal 2 samples the measured $\delta^{13}C_{OC}$ values of the ambient particles were distributed between the mentioned $\delta^{13}C_{TC}$ values of the main OA sources. Smaller particles (D_{50} up to 0.18 μm) possessed depleted $\delta^{13}C_{OC}$ values when compared to larger particles (D_{50} up to 1 μm). This is also consistent with the fact that FF combustion usually emits smaller aerosol particles than biomass burning. There were two extreme cases: the first was more refractory OC in the larges size range ($0.32 < D_{50} < 1$ μm), with isotope ratios in the range of biomass (coal) burning emissions, and the second was less refractory OC in the smallest size range $D_{50} < 180$ nm, with isotope ratios in the range of pure fossil fuel emissions. OC in more refractory small particles, less refractory large particles and all particles of intermediate size contain a mixture of these two sources. This shows that sources of OA do not only change with particle size, but also that different OA volatility fractions can be attributed to different source mixes.

The isotopic composition of OC in the coastal 1 samples differs from that of the coastal 2 samples, especially for the $0.32 < D_{50} < 1$ μm size range, where $\delta^{13}C_{OC}$was depleted by more than by 4‰ in coastal 1 samples relative to the coastal 2 samples. This strongly suggests that the shipping related source identified has strongly depleted isotopic signature. The most negative stable carbon isotopic values (−30.9) give a strong indication of advected pollution from Klaipeda harbour, potentially consisting of unburnt fossil fuel components (e.g., raw fuel storage tanks ate the harbour).

Fig. 6 shows the van Krevelen diagram (plot of the atomic ratios O/C versus H/C) averaged for the different size and volatility classes. The individual data for each impactor stage and desorption temperature are shown in Fig. S4. The O/C ratios of the more refractory OA fraction were variable and also varied with particle size. Moreover, they showed a strong inverse correlation with H/C ratios (slope −1). This is usually explained by oxidative processing and gives an indication that the more refractory carbon fraction is chemically more processed. During this winter-time campaigns it might also be an indication of mixing of two principal sources (biomass burning and fossil fuel combustion) that could adequately represent variation in more and less refractory material. However, it is not clear, if this would lead to a slope of −1. Less refractory samples show distinct O/C ratios at different sites (i.e. O/C ratios between 0.2 and 0.26 at coastal 1, between 0.3 and 0.31 at coastal 2 and between 0.34 and 0.36 at city), which indicates that the less refractory OC is probably more local in origin. In contrary the O/C ratios of the more refractory OM show significant overlap in samples from the different sites (Fig. 6), which is an indication that the more refractory OC is less local and more regionally distributed. For the less refractory OM fraction, O/C and H/C ratios vary within a relatively narrow range in coastal 2 and urban samples, which indicate that they are probably less chemically processed than more refractory particles. For coastal 1 there is an inverse relationship between O/C and H/C in the less refractory OA, but with a slope different from 1. In this case this is probably caused by the influence of the local source with a high mass fraction of heavy hydrocarbons, which was the most pronounced in the large particle fraction. This can cause the high H/C and low O/C ratios observed in less refractory, large particles in coastal 1 (Fig. 6).

O/C ratios were variable and ranged from 0.20 to 0.45 between volatility classes and sites. Such range can cover multiple sources such as biomass burning (O/C) (Heringa et al., 2011), biogenic SOA (Faiola et al., 2015) or even aerosol aging (Ng et al., 2011). It is possible that the less refractory OC is partially of secondary origin. Secondary OC that condenses onto aerosol particles is expected to be depleted in ^{13}C (Wang and Kawamura, 2006; Fisseha et al., 2009b) and it desorbs largely at 100 and 150 °C (Meusinger et al., 2017). A higher fraction of secondary OC could be the reason why during the coastal 2 period more of the OC desorbed at low desorption temperatures (100 and 150 °C) (Fig S3). Secondary formation would also explain that the $\delta^{13}C$ values of less refractory OC were more negative in coastal 2 than in urban samples (Table 2, Fig. 5) and that OC and TC $\delta^{13}C$ ratios differed more strongly than at the urban site (Table 2).

Another possible process that could change the $\delta^{13}C$ is photochemical processing. Prolonged photochemical processing usually leads to a more oxidized, isotopically enriched OA. Evidence for this process is usually found at remote receptor sites (Kirillova et al., 2014; Masalaite et al., 2017). In this data set, there is evidence of oxidative processing of the more refractory OA fraction based on the inverse relationship between O/C and H/C ratios. A scatter plot of $\delta^{13}C$ ratios versus the atomic ratios of O/C (Fig. 7) shows very

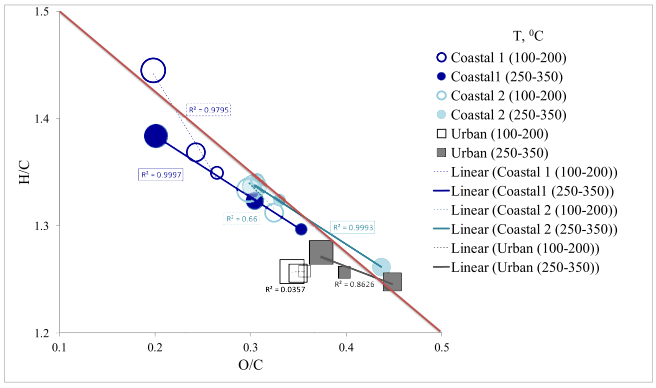

Fig. 6. Van Krevelen diagram of two desorption temperature ranges (100–200, 250–350) at coastal and urban sites. The size of the symbol is proportional to the particle size range ($D_{50} < 0.18$ μm, $0.18 < D_{50} < 0.32$ μm and $0.32 < D_{50} < 1$ μm, respectively).

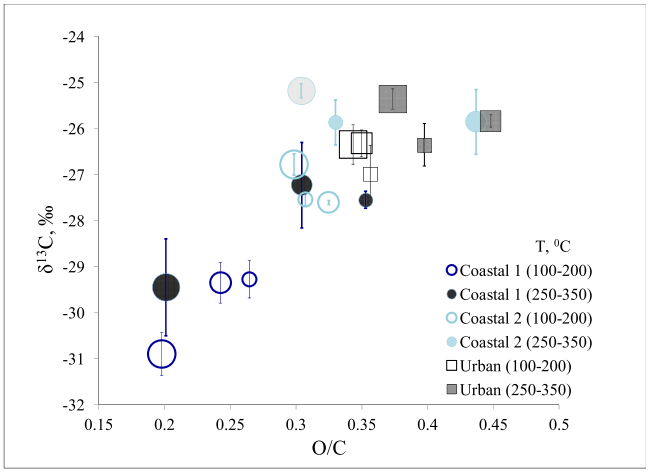

Fig. 7. The isotopic composition of OC via the atomic ratios of O/C at urban (squares) and coastal (circles) sites for size segregated aerosol particles in two desorption temperature ranges (100–200, 250–350). The size of the symbol is proportional to particle size range ($D_{50} < 0.18$ μm, $0.18 < D_{50} < 0.32$ μm and $0.32 < D_{50} < 1$ μm, respectively). Error bars correspond to the standard deviation of mean of the samples averaged for each period.

clearly that the low oxidation level for several OC fractions in coastal 1 is associated with the most negative $\delta^{13}C_{OC}$ values (coastal 1 (100–200 °C) data). The most oxidized particles exhibit more enriched $\delta^{13}C_{OC}$ values (urban (250–350 °C)) in comparison to the coastal 1 period. The correlation of $\delta^{13}C_{OC}$ and O/C in less refractory OM observed in coastal 1 samples is most likely not a results of oxidative processing: CH_{PTR} (the fraction of hydrocarbon in all OA_{PTR}) and $\delta^{13}C_{OC}$ values of less refractory OA also show a strong negative correlation for coastal 1 samples ($r = -0.999$; $p = 0.02$ at 100–200 °C), which suggests that the variation in $\delta^{13}C_{OC}$ and O/C are both caused by variable contributions of an isotopically depleted fossil fuel source.

In the coastal 2 and urban samples, there is no clear relationship between $\delta^{13}C_{OC}$ and O/C ratio, where enriched $\delta^{13}C$ values are associated with higher O/C ratios. This might be due to variable direct source contribution or relatively complex oxidation chemistry. In the latter case the less refractory OA could contain a mixture of (depleted) reaction products, as well as parent compounds for further reactions, which would not lead to a clear correlation with $\delta^{13}C$. It is in line with (Masalaite et al., 2017), which found clear correlations of O/C ratios and $\delta^{13}C_{OC}$ only at a remote forest site. This indicates that the oxidative processing implied by the Van Krevelen diagram does not result in a clear isotopic signature and the enriched $\delta^{13}C$ values are most likely caused by a higher contribution of biomass burning to the urban OM.

4. Conclusions

Chemical and isotopic analysis of carbonaceous aerosol particles collected at the coastal site revealed two periods with strongly different OC properties: coastal 1 and coastal 2. A new source was identified that manifested itself in $0.32 < D_{50} < 1$ μm size range composed of hydrocarbons (25%), high number of heavy ($m/z > 200$), low volatile (desorption temperature 250–350 °C) particles and the most negative $\delta^{13}C_{OC}$ values that reached up to −31‰ in the coastal 1 case strongly linked to the shipping emissions according to PTR mass spectral analysis.

There was a clear distinction in source contribution between the less refractory OC fraction and the more refractory fraction during coastal 2 period and the urban site. According to the source apportionment method used in this study, the less refractory carbon fraction of the smallest particles was almost entirely originating from fossil fuels, whereas the more refractory carbon fraction in the large size range was largely originating from biomass burning. The more refractory small particles and the less refractory large particles were roughly of even proportions originating from the above sources.

Clear differences in O/C and H/C ratios as well $\delta^{13}C$ values between the two sampling sites, indicated a more local character of less refractory OA, whereas more refractory OA seems to be more regionally produced. A negative correlation between H/C and O/C ratios for the more refractory OA gives evidence of atmospheric processing of the more refractory OA. There is no significant correlation between O/C and $\delta^{13}C$ for the more refractory carbon fraction, which probably indicates that the isotopic signature is governed more by source signatures than by fractionation due to chemical reactions. This is consistent with diminished photochemistry and SOA formation during the winter.

In summary, varying contributions of fossil fuel combustion and biomass burning sources as well as SOA formation could explain the difference in $\delta^{13}C$ between the more and less refractory OA. SOA formation is probably less important at the urban site and more important for the coastal 2 samples. More refractory OA during the coastal 1 period are likely of primary origin and associated with shipping emissions based on their low O/C ratio, high H/C ratio, the most negative $\delta^{13}C_{OC}$ values and characteristic mass spectra.

Acknowledgements

Postdoctoral fellowship of A. Masalaite was funded by the European Union Structural Fund project “Postdoctoral Fellowship Implementation in Lithuania”. This study was funded by the Dutch Science Foundation (NWO grants Nr. 820.01.001, and 824.14.002).

Appendix A. Supplementary data

Supplementary data related to this article can be found at https://doi.org/10.1016/j.envpol.2018.04.073.

References

Al-Naiema, I.M., Stone, E.A., 2017. Evaluation of anthropogenic secondary organic aerosol tracers from aromatic hydrocarbons. Atmos. Chem. Phys. 17, 2053–2065.

Ballentine, D.C., Macko, S.A., Turekian, V.C., 1998. Variability of stable carbon isotopic compositions in individual fatty acids from combustion of C 4 and C 3 plants: implications for biomass burning. Chem. Geol. 152, 151–161.

Bikkina, S., Kawamura, K., Sarin, M., 2016. Stable carbon and nitrogen isotopic composition of fine mode aerosols (PM 2.5) over the Bay of Bengal: impact of continental sources. Tellus B 68.

Bozzetti, C., Daellenbach, K.R., Hueglin, C., Fermo, P., Sciare, J., Kasper-Giebl, A., Mazar, Y., Abbaszade, G. l, El Kazzi, M., Gonzalez, R., 2016. Size-resolved identification, characterization, and quantification of primary biological organic aerosol at a european rural site. Environ. Sci. Technol. 50, 3425–3434.

Cachier, H., Buat-Menard, P., Fontugne, M., Rancher, J., 1985. Source terms and source strengths of the carbonaceous aerosol in the tropics. J. Atmos. Chem. 3, 469–489.

Cao, F., Zhang, S.-C., Kawamura, K., Zhang, Y.-L., 2016. Inorganic markers, carbonaceous components and stable carbon isotope from biomass burning aerosols in Northeast China. Sci. Total Environ. 572, 1244–1251. https://doi.org/10.1016/j.scitotenv.2015.09.099.

Cao, J.-j., Chow, J.C., Tao, J., Lee, S.-c., Watson, J.G., Ho, K.-f., Wang, G.-h., Zhu, C.-s., Han, Y.-m., 2011. Stable carbon isotopes in aerosols from Chinese cities: influence of fossil fuels. Atmos. Environ. 45, 1359–1363.

Ceburnis, D., Garbaras, A., Szidat, S., Rinaldi, M., Fahrni, S., Perron, N., Wacker, L., Leinert, S., Remeikis, V., Facchini, M., 2011. Quantification of the carbonaceous matter origin in submicron marine aerosol by 13 C and 14 C isotope analysis. Atmos. Chem. Phys. 11, 8593–8606.

Ceburnis, D., Masalaite, A., Ovadnevaite, J., Garbaras, A., Remeikis, V., Maenhaut, W., Claeys, M., Sciare, J., Baisnée, D., O'Dowd, C.D., 2016. Stable isotopes measurements reveal dual carbon pools contributing to organic matter enrichment in marine aerosol. Sci. Rep. 6.

Collier, S., Zhou, S., Kuwayama, T., Forestieri, S., Brady, J., Zhang, M., Kleeman, M., Cappa, C., Bertram, T., Zhang, Q., 2015. Organic PM emissions from vehicles: composition, O/C ratio, and dependence on PM concentration. Aerosol. Sci. Technol. 49, 86–97.

Davidson, C.I., Phalen, R.F., Solomon, P.A., 2005. Airborne particulate matter and human health: a review. Aerosol. Sci. Technol. 39, 737–749.

Di Natale, F., Carotenuto, C., 2015. Particulate matter in marine diesel engines exhausts: Emissions and control strategies. Transport. Res. D Transport Environ. 40, 166–191.

Dusek, U., Meusinger, C., Oyama, B., Ramon, W., de Wilde, P., Holzinger, R., Röckmann, T., 2013. A thermal desorption system for measuring δ 13 C ratios on organic aerosol. J. Aerosol Sci. 66, 72–82.

Eichler, P., Müller, M., Rohmann, C., Stengel, B., Orasche, J. r., Zimmermann, R., Wisthaler, A., 2017. Lubricating oil as a major constituent of ship exhaust particles. Environ. Sci. Technol. Lett. 4, 54–58.

Faiola, C., Wen, M., VanReken, T., 2015. Chemical characterization of biogenic secondary organic aerosol generated from plant emissions under baseline and stressed conditions: inter-and intra-species variability for six coniferous species. Atmos. Chem. Phys. 15, 3629–3646.

Fisseha, R., Saurer, M., Jäggi, M., Siegwolf, R.T., Dommen, J., Szidat, S., Samburova, V., Baltensperger, U., 2009a. Determination of primary and secondary sources of organic acids and carbonaceous aerosols using stable carbon isotopes. Atmos. Environ. 43, 431–437.

Fisseha, R., Spahn, H., Wegener, R., Hohaus, T., Brasse, G., Wissel, H., Tillmann, R., Wahner, A., Koppmann, R., Kiendler-Scharr, A., 2009b. Stable carbon isotope composition of secondary organic aerosol from β-pinene oxidation. J. Geophys. Res.: Atmosphere 114.

Garbaras, A., Andriejauskiene, J., Bariseviciute, R., Remeikis, V., 2008. Tracing of atmospheric aerosol sources using stable carbon isotopes. Lithuanian J. Phys. 48, 259–264.

Garbaras, A., Masalaite, A., Garbariene, I., Ceburnis, D., Krugly, E., Remeikis, V., Puida, E., Kvietkus, K., Martuzevicius, D., 2015. Stable carbon fractionation in size-segregated aerosol particles produced by controlled biomass burning.

J. Aerosol Sci. 79, 86–96. https://doi.org/10.1016/j.jaerosci.2014.10.005.
Garbarienė, I., Šapolaitė, J., Garbaras, A., Ežerinskis, Ž., Poceviˇcius, M., Krikščikas, L., Plukis, A., Remeikis, V., 2016. Origin identification of carbonaceous aerosol particles by carbon isotope ratio analysis. Aerosol Air Qual. Res. 16, 1356–1365.
Gensch, I., Kiendler-Scharr, A., Rudolph, J., 2014. Isotope ratio studies of atmospheric organic compounds: principles, methods, applications and potential. Int. J. Mass Spectrom. 365, 206–221.
GoogleMaps, 2016. Moudi Samples Collection and Wind Data Collection Sites. Google. https://www.google.lt/maps/@54.8608858,15.7139035,4.83z.
Górka, M., Jędrysek, M.-O., 2008. d 13 C of organic atmospheric dust deposited in Wrocław (SW Poland): critical remarks on the passive method. Geol. Q. 52, 115–126.
Górka, M., Rybicki, M., Simoneit, B.R., Marynowski, L., 2014. Determination of multiple organic matter sources in aerosol PM 10 from Wrocław, Poland using molecular and stable carbon isotope compositions. Atmos. Environ. 89, 739–748.
Hegde, P., Kawamura, K., Joshi, H., Naja, M., 2016. Organic and inorganic components of aerosols over the central Himalayas: winter and summer variations in stable carbon and nitrogen isotopic composition. Environ. Sci. Pollut. Res. 23, 6102–6118.
Hellén, H., Dommen, J., Metzger, A., Gascho, A., Duplissy, J., Tritscher, T., Prevot, A.S., Baltensperger, U., 2008. Using proton transfer reaction mass spectrometry for online analysis of secondary organic aerosols. Environ. Sci. Technol. 42, 7347–7353.
Heringa, M., DeCarlo, P., Chirico, R., Tritscher, T., Dommen, J., Weingartner, E., Richter, R., Wehrle, G., Prévôt, A., Baltensperger, U., 2011. Investigations of primary and secondary particulate matter of different wood combustion appliances with a high-resolution time-of-flight aerosol mass spectrometer. Atmos. Chem. Phys. 11, 5945–5957.
Holzinger, R., Kasper-Giebl, A., Staudinger, M., Schauer, G., Röckmann, T., 2010a. Analysis of the chemical composition of organic aerosol at the Mt. Sonnblick observatory using a novel high mass resolution thermal-desorption proton-transfer-reaction mass-spectrometer (hr-TD-PTR-MS). Atmos. Chem. Phys. 10, 10111–10128.
Holzinger, R., Williams, J., Herrmann, F., Lelieveld, J., Donahue, N., Röckmann, T., 2010b. Aerosol analysis using a Thermal-Desorption Proton-Transfer-Reaction Mass Spectrometer (TD-PTR-MS): a new approach to study processing of organic aerosols. Atmos. Chem. Phys. 10, 2257–2267.
Holzinger, R., Goldstein, A., Hayes, P., Jimenez, J., Timkovsky, J., 2013. Chemical evolution of organic aerosol in Los Angeles during the CalNex 2010 study. Atmos. Chem. Phys. 13, 10125–10141.
Holzinger, R., 2015. PTRwid: a new widget-tool for processing PTR-TOF-MS data. Atmos. Meas. Tech. Discuss. 8, 1629–1669.
Hueglin, C., Gehrig, R., Baltensperger, U., Gysel, M., Monn, C., Vonmont, H., 2005. Chemical characterisation of PM2. 5, PM10 and coarse particles at urban, near-city and rural sites in Switzerland. Atmos. Environ. 39, 637–651.
IBM, 2013. IBM SPSS Statistics for Windows. IBM Corp., Armonk, NY, Version 22.0.
Inomata, S., Sato, K., Hirokawa, J., Sakamoto, Y., Tanimoto, H., Okumura, M., Tohno, S., Imamura, T., 2014. Analysis of secondary organic aerosols from ozonolysis of isoprene by proton transfer reaction mass spectrometry. Atmos. Environ. 97, 397–405.
Jimenez, J., Canagaratna, M., Donahue, N., Prevot, A., Zhang, Q., Kroll, J.H., DeCarlo, P.F., Allan, J.D., Coe, H., Ng, N., 2009. Evolution of organic aerosols in the atmosphere. Science 326, 1525–1529.
Kaufman, Y.J., Tanré, D., Boucher, O., 2002. A satellite view of aerosols in the climate system. Nature 419, 215–223.
Kawamura, K., Kobayashi, M., Tsubonuma, N., Mochida, M., Watanabe, T., Lee, M., 2004. Organic and inorganic compositions of marine aerosols from East Asia: seasonal variations of water-soluble dicarboxylic acids, major ions, total carbon and nitrogen, and stable C and N isotopic composition. Geochem. Soc. Special Publ. 9, 243–265.
Kirchstetter, T.W., Novakov, T., 2007. Controlled generation of black carbon particles from a diffusion flame and applications in evaluating black carbon measurement methods. Atmos. Environ. 41, 1874–1888.
Kirillova, E.N., Andersson, A., Sheesley, R.J., Kruså, M., Praveen, P., Budhavant, K., Safai, P., Rao, P., Gustafsson, Ö., 2013. 13C-and 14C-based study of sources and atmospheric processing of water-soluble organic carbon (WSOC) in South Asian aerosols. J. Geophys. Res. Atmos. 118, 614–626.
Kirillova, E.N., Andersson, A., Tiwari, S., Srivastava, A.K., Bisht, D.S., Gustafsson, Ö., 2014. Water-soluble organic carbon aerosols during a full New Delhi winter: isotope-based source apportionment and optical properties. J. Geophys. Res. Atmos. 119 (6), 3476–3485.
Kundu, S., Kawamura, K., Andreae, T.W., Hoffer, A., Andreae, M.O., 2010. Diurnal variation in the water-soluble inorganic ions, organic carbon and isotopic compositions of total carbon and nitrogen in biomass burning aerosols from the LBA-SMOCC campaign in Rondônia, Brazil. J. Aerosol Sci. 41, 118–133.
Lambe, A.T., Miracolo, M.A., Hennigan, C.J., Robinson, A.L., Donahue, N.M., 2009. Effective rate constants and uptake coefficients for the reactions of organic molecular markers (n-Alkanes, hopanes, and steranes) in motor oil and diesel primary organic aerosols with hydroxyl radicals. Environ. Sci. Technol. 43, 8794–8800.
Masalaite, A., Garbaras, A., Remeikis, V., 2012. Stable isotopes in environmental investigations. Lithuanian J. Phys. 52, 261–268.
Masalaite, A., Remeikis, V., Garbaras, A., Dudoitis, V., Ulevicius, V., Ceburnis, D., 2015. Elucidating carbonaceous aerosol sources by the stable carbon δ 13 C TC ratio in size-segregated particles. Atmos. Res. 158, 1–12.
Masalaite, A., Holzinger, R., Remeikis, V., Röckmann, T., Dusek, U., 2017. Characteristics, sources and evolution of fine aerosol (PM 1) at urban, coastal and forest background sites in Lithuania. Atmos. Environ. 148, 62–76.
Meusinger, C., Dusek, U., King, S.M., Holzinger, R., Rosenørn, T., Sperlich, P., Julien, M., Remaud, G.S., Bilde, M., Röckmann, T., 2017. Chemical and isotopic composition of secondary organic aerosol generated by α-pinene ozonolysis. Atmos. Chem. Phys. 17, 6373–6391.
Mordas, G., Sipilä, M., Kulmala, M., 2008. Nanometer particle detection by the condensation particle counter UF-02proto. Aerosol. Sci. Technol. 42, 521–527.
Narukawa, M., Kawamura, K., Takeuchi, N., Nakajima, T., 1999. Distribution of dicarboxylic acids and carbon isotopic compositions in aerosols from 1997 Indonesian forest fires. Geophys. Res. Lett. 26, 3101–3104.
Ng, N., Canagaratna, M., Jimenez, J., Chhabra, P., Seinfeld, J., Worsnop, D., 2011. Changes in organic aerosol composition with aging inferred from aerosol mass spectra. Atmos. Chem. Phys. 11, 6465–6474.
Oyama, B.S., Andrade, M. d. F., Herckes, P., Dusek, U., Röckmann, T., Holzinger, R., 2016. Chemical characterization of organic particulate matter from on-road traffic in São Paulo, Brazil. Atmos. Chem. Phys. 16, 14397–14408.
Pavuluri, C.M., Kawamura, K., 2012. Evidence for 13-carbon enrichment in oxalic acid via iron catalyzed photolysis in aqueous phase. Geophys. Res. Lett. 39.
Pérez, N., Pey, J., Querol, X., Alastuey, A., López, J., Viana, M., 2008. Partitioning of major and trace components in PM 10–PM 2.5–PM 1 at an urban site in Southern Europe. Atmos. Environ. 42, 1677–1691.
Putaud, J.-P., Van Dingenen, R., Alastuey, A., Bauer, H., Birmili, W., Cyrys, J., Flentje, H., Fuzzi, S., Gehrig, R., Hansson, H.-C., 2010. A European aerosol phenomenology–3: physical and chemical characteristics of particulate matter from 60 rural, urban, and kerbside sites across Europe. Atmos. Environ. 44, 1308–1320.
Ren, L., Fu, P., He, Y., Hou, J., Chen, J., Pavuluri, C.M., Sun, Y., Wang, Z., 2016. Molecular distributions and compound-specific stable carbon isotopic compositions of lipids in wintertime aerosols from Beijing. Sci. Rep. 6, 27481.
Röckmann, T., Kaiser, J., Brenninkmeijer, C.A., Brand, W.A., 2003. Gas chromatography/isotope-ratio mass spectrometry method for high-precision position-dependent 15N and 18O measurements of atmospheric nitrous oxide. Rapid Commun. Mass Spectrom. 17, 1897–1908.
Rogula-Kozłowska, W., Klejnowski, K., Rogula-Kopiec, P., Ośródka, L., Krajny, E., Błaszczak, B., Mathews, B., 2014. Spatial and seasonal variability of the mass concentration and chemical composition of PM2. 5 in Poland. Air Qual. Atmos. Health 7, 41–58.
Saccon, M., Kornilova, A., Huang, L., Moukhtar, S., Rudolph, J., 2015. Stable carbon isotope ratios of ambient secondary organic aerosols in Toronto. Atmos. Chem. Phys. 15, 10825–10838.
Sang, X., Gensch, I., Kammer, B., Khan, A., Kleist, E., Laumer, W., Schlag, P., Schmitt, S., Wildt, J., Zhao, R., 2016. Chemical stability of levoglucosan: an isotopic perspective. Geophys. Res. Lett. 43 (10), 5419–5424.
Sang, X.F., Gensch, I., Laumer, W., Kammer, B., Chan, C.Y., Engling, G., Wahner, A., Wissel, H., Kiendler-Scharr, A., 2012. Stable carbon isotope ratio analysis of anhydrosugars in biomass burning aerosol particles from source samples. Environ. Sci. Technol. 46, 3312–3318.
Squizzato, S., Masiol, M., Agostini, C., Visin, F., Formenton, G., Harrison, R.M., Rampazzo, G., 2016. Factors, origin and sources affecting PM 1 concentrations and composition at an urban background site. Atmos. Res. 180, 262–273.
Stein, A., Draxler, R., Rolph, G., Stunder, B., Cohen, M., Ngan, F., 2015. NOAA's HYSPLIT atmospheric transport and dispersion modeling system. Bull. Am. Meteorol. Soc. 96, 2059–2077.
Timkovsky, J., Dusek, U., Henzing, J.S., Kuipers, T.L., Röckmann, T., Holzinger, R., 2015. Offline thermal-desorption proton-transfer-reaction mass spectrometry to study composition of organic aerosol. J. Aerosol Sci. 79, 1–14. https://doi.org/10.1016/j.jaerosci.2014.08.010.
Ulevicius, V., Byčenkienė, S., Bozzetti, C., Vlachou, A., Plauškaitė, K., Mordas, G., Dudoitis, V., Abbaszade, G., Remeikis, V., Garbaras, A., Masalaite, A., Blees, J., Fröhlich, R., Dällenbach, K., Canonaco, F., Slowik, J., Dommen, J., Zimmermann, R., Schnelle-Kreis, J., Salazar, G., Agrios, K., Szidat, S., Haddad, E., Prévôt, A., 2016. Fossil and non-fossil source contributions to atmospheric carbonaceous aerosols during extreme spring grassland fires in Eastern Europe. Atmos. Chem. Phys. 16, 5513–5529.
Viana, M., Hammingh, P., Colette, A., Querol, X., Degraeuwe, B., de Vlieger, I., van Aardenne, J., 2014. Impact of maritime transport emissions on coastal air quality in Europe. Atmos. Environ. 90, 96–105.
Virkkula, A., Mäkelä, T., Hillamo, R., Yli-Tuomi, T., Hirsikko, A., Hämeri, K., Koponen, I.K., 2007. A simple procedure for correcting loading effects of aethalometer data. J. Air Waste Manag. Assoc. 57, 1214–1222.
Wang, H., Kawamura, K., 2006. Stable carbon isotopic composition of low-molecular-weight dicarboxylic acids and ketoacids in remote marine aerosols. J. Geophys. Res.: Atmosphere 111.
Weingartner, E., Saathoff, H., Schnaiter, M., Streit, N., Bitnar, B., Baltensperger, U., 2003. Absorption of light by soot particles: determination of the absorption coefficient by means of aethalometers. J. Aerosol Sci. 34, 1445–1463.
Widory, D., 2006. Combustibles, fuels and their combustion products: a view through carbon isotopes. Combust. Theor. Model. 10, 831–841.
Wiedensohler, A., 1988. An approximation of the bipolar charge distribution for particles in the submicron size range. J. Aerosol Sci. 19, 387–389.
Wiedensohler, A., Birmili, W., Nowak, A., Sonntag, A., Weinhold, K., Merkel, M., Wehner, B., Tuch, T., Pfeifer, S., Fiebig, M., 2012. Mobility particle size

spectrometers: harmonization of technical standards and data structure to facilitate high quality long-term observations of atmospheric particle number size distributions. Atmos. Meas. Tech. 5, 657–685.
Worton, D.R., Isaacman, G., Gentner, D.R., Dallmann, T.R., Chan, A.W., Ruehl, C., Kirchstetter, T.W., Wilson, K.R., Harley, R.A., Goldstein, A.H., 2014. Lubricating oil dominates primary organic aerosol emissions from motor vehicles. Environ. Sci. Technol. 48, 3698–3706.
Zhang, Y.L., Kawamura, K., Cao, F., Lee, M., 2016. Stable carbon isotopic compositions of low-molecular-weight dicarboxylic acids, oxocarboxylic acids, α-dicarbonyls, and fatty acids: implications for atmospheric processing of organic aerosols. J. Geophys. Res. Atmos. 121, 3707–3717.